Random Kondo alloys investigated with the coherent potential approximation

S. Burdin and P. Fulde
Max Planck Institut für Physik Komplexer Systeme, Nöthnitzer Strasse 38, 01187 Dresden, Germany
(Received 25 January 2007; revised manuscript received 26 July 2007; published 24 September 2007)

The interplay between the Kondo effect and disorder is studied. This is done by applying a matrix coherent potential approximation and treating the Kondo interaction on a mean-field level. The resulting equations are shown to agree with those derived by the dynamical mean-field theory. By applying the formalism to a Bethe tree structure with infinite coordination, the effects of diagonal and off-diagonal disorder are studied. Special attention is paid to the behavior of the Kondo and the Fermi-liquid temperature as function of disorder and concentration of the Kondo ions. The nonmonotonous dependence of these quantities is discussed.

DOI: 10.1103/PhysRevB.76.104425 PACS number(s): 75.20.Hr, 71.10.Fd, 71.27.+a, 75.30.Mb

I. INTRODUCTION

The Kondo effect is one of the most investigated phenomena in solid-state physics. Part of the reason is that it cannot be treated perturbationally since it is a strong coupling effect. Therefore, it requires special theoretical tools to deal with it. Kondo physics occurs when strongly correlated electrons such as $4f$ electrons in Ce^{3+} or holes in Yb^{3+} are weakly hybridizing with the conduction electrons of their surroundings. This results in low-energy excitations which in the case of concentrated systems may result in heavy quasiparticles. For recent reviews of the field, we refer to Refs. 1–3. A realistic starting point for Kondo systems is the Anderson impurity or Anderson lattice model. Due to the hybridization mentioned above it involves spin as well as charge degrees of freedom. Often the charge degrees of freedom are less interesting and are therefore eliminated by a Schrieffer-Wolf transformation.[4] The result is an antiferromagnetic interaction between the spins of the conduction electrons and the strongly correlated localized, e.g., $4f$ electrons. This leads to the Kondo Hamiltonian.

Competing with the Kondo effect is the Ruderman-Kittel-Kasuya-Yosida (RKKY) interaction. While the Kondo effect leads to the formation of a singlet between the spins of the $4f$ and conduction electrons, the RKKY interaction lowers the energy of a system of local spins interacting with each other via conduction electrons. Therefore, if the latter is more important than the former, the local spins will remain uncompensated and eventually order and do not participate in the singlet formation.

The aim of the present investigation is to study the effect of randomness on Kondo physics. It has been suggested in several works that randomness and disorder lead to non-Fermi-liquid (NFL) behavior at low temperatures.[5–12] For example, it has been shown in Refs. 5–7 that a distribution of Kondo temperatures T_K can result from local disorder, the NFL features being related to the presence of very-low-T_K spins which remain unquenched at any finite temperature. In Refs. 5–8, the systems are modeled by introducing a continuous distribution of local energy levels or electronic exchange. Here, we consider a discrete distribution of disorder, and assume that the system is characterized by two different kinds of sites only.

Another possible scenario attributes the NFL behavior to the proximity to a quantum critical point resulting from disordered RKKY interactions.[9–11] More recently, it has been suggested that a NFL behavior can occur between the local Fermi-liquid (FL) and coherent heavy FL phases characterizing, respectively, a dilute and a dense Kondo alloy.[12]

We assume that we are in a regime where the Kondo effect is more important than the RKKY interaction so that the latter may be neglected. Instead we concentrate on the singlet formation energy and on how it can be expressed in terms of the Kondo temperature T_K and of the temperature T_{FL} which determines the low temperature thermodynamic properties. More precisely we compute the behavior of a temperature T_0 defined by the inverse local susceptibility at zero temperature $\chi_{\mathrm{loc}}^{-1}(T=0)$ which is often identified with T_{FL}. In particular, we study how T_K and T_0 behave as functions of conduction electron band filling n_c, local spin concentration x, and disorder.

II. MODEL HAMILTONIAN AND METHODS OF SOLUTIONS

We consider the Kondo-alloy model (KAM) with the Hamiltonian

$$H=\sum_{ij\sigma} t_{ij}c_{i\sigma}^{\dagger}c_{j\sigma}+\frac{J_K}{2}\sum_{i\in A}\sum_{\sigma\sigma'}\mathbf{S}_i\cdot\boldsymbol{\sigma}_i, \tag{1}$$

where the first term describes nearest-neighbor hopping of conduction electrons on a lattice with sites occupied randomly by atoms of kind A and B. The corresponding concentrations are $c_A=x$ and $c_B=1-x$. The hopping matrix elements have three different values, i.e.,

$$t_{ij}=\gamma_{ij}\begin{cases} t_A & \text{if } i,j\in A \\ t_B & \text{if } i,j\in B \\ t_{AB} & \text{otherwise.}\end{cases} \tag{2}$$

Here γ_{ij} is the structure factor of the underlying periodic lattice with Fourier transform $\gamma_{\mathbf{k}}\equiv\Sigma_{ij}\gamma_{ij}\exp i\mathbf{k}\cdot(\mathbf{R}_j-\mathbf{R}_i)$. The second term in Eq. (1) describes the Kondo interaction between the conduction electron spin and local spin operators $\mathbf{S}_i$, the latter being attached to atoms of type A only.

We shall treat the Kondo-alloy model defined by Eq. (1) by applying a number of approximations. A rather simple one is that we assume a random distribution of sites A and B.

As regards the Kondo interaction we shall consider two different ways of treating the randomness. They are similar to each other but based on different physical pictures.

One approach is a generalization of a coherent potential approximation (CPA) matrix approach originally introduced in Refs. 13 and 14. The Kondo interaction is treated here within a mean-field approximation. The second approach is a matrix generalization of the dynamical mean-field theory (DMFT) which is exact in the limit of infinite dimensions.[15,16] Averaging over the randomness is done here without simplifying the Kondo interaction. A mean-field approximation can be introduced before or after the DMFT approximation and leads to the same set of self-consistent equations as obtained in the first, i.e., the generalized CPA approach.

The analytical expressions obtained from these two approaches are applicable to any lattice structure. The numerical results presented below apply the DMFT to a Bethe lattice instead of a regular one. The Kondo interaction is treated in this case within the mean-field approximation.

III. MATRIX COHERENT POTENTIAL APPROXIMATION METHOD

A. Mean-field treatment of the Kondo interaction

We begin with a mean-field approximation for the Kondo interaction. Following the standard theory,[17–21] the spin operators are written in fermionic representation $\mathbf{S}_i^{\sigma\sigma'}=f_{i\sigma}^{\dagger}f_{i\sigma'}-\delta_{\sigma\sigma'}/2$, with the constraint $\Sigma_\sigma f_{i\sigma}^{\dagger}f_{i\sigma}=1$. The Hamiltonian equation (1) becomes therefore

$$H=\sum_{ij\sigma}t_{ij}c_{i\sigma}^{\dagger}c_{j\sigma}+\frac{J_K}{2}\sum_{i\in A}\sum_{\sigma\sigma'}f_{i\sigma}^{\dagger}f_{i\sigma'}c_{i\sigma'}^{\dagger}c_{i\sigma}. \tag{3}$$

The systems we want to describe here involve physical spins 1/2 with a $SU(2)$ symmetry. The mean-field approach as introduced in Refs. 17 and 18 is in this case an approximation which becomes exact in the limit of $SU(N\to\infty)$ symmetry.[19–21] The Hamiltonian is

$$H=\sum_{ij\sigma}t_{ij}c_{i\sigma}^{\dagger}c_{j\sigma}-r\sum_{\sigma}\sum_{i\in A}(c_{i\sigma}^{\dagger}f_{i\sigma}+f_{i\sigma}^{\dagger}c_{i\sigma})$$
$$-\mu\sum_{\sigma}\sum_{i}\left(c_{i\sigma}^{\dagger}c_{i\sigma}-\frac{n_c}{2}\right)-\lambda\sum_{\sigma}\sum_{i\in A}\left(f_{i\sigma}^{\dagger}f_{i\sigma}-\frac{1}{2}\right), \tag{4}$$

where n_c is the average number of conduction electrons per site i, while μ denotes the chemical potential. In the following, we discard the spin index σ since in mean-field approximation the contributions to H of the different spin components decouple.[17–21] The Kondo interaction is approximated by an effective hybridization $r=-J_K[\langle f_i c_i^{\dagger}\rangle]$ between the conduction electrons and the fermionic operators, where the $\langle\cdots\rangle$ denotes the thermal average with respect to the Hamiltonian (4) for random configurations of sites A and B, and $[\cdots]$ denotes the average with respect to these configurations. Note that the same form of the Hamiltonian is obtained by starting from an Anderson lattice instead of a Kondo lattice, and treating it within the mean-field slave boson approximation.[19–21] We have started here from the Kondo Hamiltonian because we are interested in the case of near integer valency of the impurity, i.e., the f electron count is supposed to be very close to one. The above mean-field approximation leads to an f-like band. It models the low-energy excitations which result from the Kondo interaction or alternatively Anderson Hamiltonian. The conditions $\Sigma_\sigma f_{i\sigma}^{\dagger}f_{i\sigma}=1$ are taken into account by Lagrange parameters λ_i. We set all of them equal to λ which implies that the above conditions are satisfied on average only. Thus small local fluctuations in the f electron count are possible here like in the Anderson model.

The quantities μ, λ, and r are determined by self-consistency conditions. For that purpose local Green's functions are introduced. They are different for magnetic sites A, nonmagnetic sites B, and for f as well as conduction electrons. The $G_{ij}^{ff}(\tau-\tau')\equiv-\langle T_\tau f_i(\tau)f_j^{\dagger}(\tau')\rangle$, $G_{ij}^{fc}(\tau-\tau')\equiv-\langle T_\tau f_i(\tau)c_j^{\dagger}(\tau')\rangle$, and $G_{ij}^{cc}(\tau-\tau')\equiv-\langle T_\tau c_i(\tau)c_j^{\dagger}(\tau')\rangle$ are finite temperature Green's functions defined for imaginary time τ, where T_τ denotes the imaginary-time chronological ordering. We also define the averaged local Green's functions

$$G_A^{ff}\equiv\frac{1}{x}\sum_{i\in A}G_{ii}^{ff},\quad G_A^{fc}\equiv\frac{1}{x}\sum_{i\in A}G_{ii}^{fc}, \tag{5}$$

$$G_A^{cc}\equiv\frac{1}{x}\sum_{i\in A}G_{ii}^{cc},\quad G_B^{cc}\equiv\frac{1}{1-x}\sum_{i\in B}G_{ii}^{cc}. \tag{6}$$

The chemical potential μ, the Lagrange multiplier λ, and the effective hybridization r are determined by the self-consistent saddle point equations as follows:

$$-r/J_K=\frac{1}{x}\sum_{i\in A}\langle f_i c_i^{\dagger}\rangle=G_A^{fc}(\tau=0^-), \tag{7}$$

$$1/2=\frac{1}{x}\sum_{i\in A}\langle f_i^{\dagger}f_i\rangle=G_A^{ff}(\tau=0^-), \tag{8}$$

$$n_c/2=\sum_{i}\langle c_i^{\dagger}c_i\rangle=G^{cc}(\tau=0^-), \tag{9}$$

with $G^{cc}\equiv\Sigma_i G_{ii}^{cc}=xG_A^{cc}+(1-x)G_B^{cc}$.

B. Configuration averages

For the determination of the Green's function of the conduction electrons, we choose a generalization of the CPA to a matrix form as introduced in Refs. 13 and 14. Within that approximation, the system can be viewed as a medium with three interacting fermionic bands: two bands corresponding to conduction electrons on sites A or B, and a third one

representing the excitations of the strongly correlated f electrons. Therefore the dynamics related to the spins of the A sites is described in a simplified form, i.e., in the form of f electrons with a dispersive band. The 3×3 Green's function matrix is of the following form:

$$\tilde{\mathbf{G}}_{ij} = \begin{pmatrix} \hat{x}_i\hat{x}_j G_{ij}^{ff} & \hat{x}_i\hat{x}_j G_{ij}^{fc} & \hat{x}_i\hat{y}_j G_{ij}^{fc} \\ \hat{x}_i\hat{x}_j G_{ij}^{cf} & \hat{x}_i\hat{x}_j G_{ij}^{cc} & \hat{x}_i\hat{y}_j G_{ij}^{cc} \\ \hat{y}_i\hat{x}_j G_{ij}^{cf} & \hat{y}_i\hat{x}_j G_{ij}^{cc} & \hat{y}_i\hat{y}_j G_{ij}^{cc} \end{pmatrix}, \tag{10}$$

where $\hat{x}_i = 1-\hat{y}_i$ are projection operators, which are unity (zero) if site i is occupied by an A (B) atom. Averaging the local Green's function matrix with respect to different configurations of randomly distributed types of atoms we find

$$[\tilde{\mathbf{G}}_{ii}] = \begin{pmatrix} xG_A^{ff} & xG_A^{fc} & 0 \\ xG_A^{cf} & xG_A^{cc} & 0 \\ 0 & 0 & (1-x)G_B^{cc} \end{pmatrix}. \tag{11}$$

In this expression, the vanishing of the mixed A-B matrix elements follows directly from $\hat{x}_i\hat{y}_i = 0$, which ensures that a given site is either of kind A or B. Averaging over the different configurations of A and B sites restores lattice translation symmetry. Therefore we define

$$\tilde{\mathbf{G}}_{\mathbf{k}} \equiv \sum_{ij} e^{-i\mathbf{k}\cdot(\mathbf{R}_i-\mathbf{R}_j)}[\tilde{\mathbf{G}}_{ij}]. \tag{12}$$

Within the single component CPA, the system is approximated by an effective medium, characterized by a local, i.e., **k**-independent, but frequency dependent self-energy.[22–26] The latter is determined self-consistently by requiring that the scattering matrix of the atoms A and B within this effective medium vanishes on average. The matrix form of the CPA introduced in Refs. 13 and 14 generalizes the scalar procedure to an effective medium with two bands of conduction electrons. Here we generalize the 2×2 matrix form of the CPA to a 3×3 one. The averaged Green's function matrix characterizing the effective medium is given by the relation

$$([\tilde{\mathbf{G}}(i\omega_n)]^{-1})_{ij} = i\omega_n\tilde{\mathbf{I}}\delta_{ij} - \mathbf{\Sigma}(i\omega_n)\delta_{ij} - \tilde{\mathbf{W}}\gamma_{ij}, \tag{13}$$

where $i\omega_n \equiv i\pi T(2n+1)$ denotes the fermionic Matsubara frequencies. In the following we leave out the n index. Invoking the reciprocal space Green's function matrix defined by Eq. (12), the relation (13) becomes

$$\tilde{\mathbf{G}}_{\mathbf{k}}^{-1}(i\omega) = i\omega\tilde{\mathbf{I}} - \tilde{\mathbf{\Sigma}}(i\omega) - \tilde{\mathbf{W}}\gamma_{\mathbf{k}}. \tag{14}$$

Here $\tilde{\mathbf{I}}$ is a 3×3 unit matrix, $\tilde{\mathbf{W}}$ is the transfer matrix,

$$\tilde{\mathbf{W}} = \begin{pmatrix} 0 & 0 & 0 \\ 0 & t_A & t_{AB} \\ 0 & t_{AB} & t_B \end{pmatrix}, \tag{15}$$

and $\tilde{\mathbf{\Sigma}}$ is a local self-energy matrix,

$$\tilde{\mathbf{\Sigma}}(i\omega) \equiv \begin{pmatrix} & \mathbf{\Sigma}_A(i\omega) & & \sigma_1(i\omega) \\ & & & \sigma_2(i\omega) \\ \sigma_1(i\omega) & & \sigma_2(i\omega) & \Sigma_B(i\omega) \end{pmatrix}, \tag{16}$$

which is determined by the set of self-consistent equations (see the Appendix) as follows:

$$[\tilde{\mathbf{G}}_{ii}(i\omega)] = \begin{pmatrix} xG_A^{ff}(i\omega) & xG_A^{fc}(i\omega) & 0 \\ xG_A^{cf}(i\omega) & xG_A^{cc}(i\omega) & 0 \\ 0 & 0 & (1-x)G_B^{cc}(i\omega) \end{pmatrix} = \sum_{\mathbf{k}} \tilde{\mathbf{G}}_{\mathbf{k}}(i\omega), \tag{17}$$

$$\mathbf{\Sigma}_A(i\omega) = -\begin{pmatrix} \lambda & r \\ r & \mu \end{pmatrix} - \frac{(1-x)}{x}\begin{pmatrix} G_A^{ff}(i\omega) & G_A^{fc}(i\omega) \\ G_A^{cf}(i\omega) & G_A^{cc}(i\omega) \end{pmatrix}^{-1}, \tag{18}$$

$$\mathbf{\Sigma}_B(i\omega) = -\mu - \frac{x}{(1-x)G_B^{cc}(i\omega)}. \tag{19}$$

The self-energies σ_1 and σ_2 are determined by requiring that the mixed A-B elements of the local Green's function matrix in Eq. (17) vanish for the same reason as in Eq. (10). We find that

$$\sigma_1(i\omega) = 0, \tag{20}$$

which reflects the fact that there is no direct interaction between f fermions and the B-electronic band, describing the electrons on nonmagnetic sites. We find also an explicit expression for σ_2, i.e.,

$$\sigma_2(i\omega) = -t_{AB}\frac{1-2x+x[i\omega+\mu-r^2/(i\omega+\lambda)]G_A^{cc}(i\omega)-(1-x)(i\omega+\mu)G_B^{cc}(i\omega)}{xt_AG_A^{cc}(i\omega)-(1-x)t_BG_B^{cc}(i\omega)}, \tag{21}$$

which results from the direct hopping of conduction electrons between A and B sites.

A complete solution of the initial Kondo-alloy system is obtained by solving simultaneously the mean-field equations (7)–(9) together with the matrix equation (17). Thereby the **k**-dependent average Green's function matrix is determined by the relation Eq. (14), with the lattice structure factor $\gamma_{\mathbf{k}}$ and the local self-energy matrix $\tilde{\mathbf{\Sigma}}$. The latter is determined by the self-consistent CPA equations (16), (18), and (19).

C. Kondo temperature

We define the Kondo temperature T_K as the temperature at which the effective hybridization r [obtained from Eqs. (7)–(9)] vanishes. We find

$$2/J_K = \int d\epsilon \rho_A^0(\epsilon+\mu_0)\tanh(\epsilon/2T_K)/\epsilon, \tag{22}$$

where ρ_A^0 and μ_0 are, respectively, the local electronic density of states (DOS) on a magnetic site, and the chemical potential of a random A-B alloy without Kondo interaction. An explicit expression for T_K has been derived in Ref. 27 in the weak-coupling regime $J_K \ll t_A$, t_B, t_{AB} as follows:

$$T_K = De^{-1/(J_K\rho_A^0(\mu_0))}\sqrt{1-(\mu_0/D)^2}F_K(n_c), \tag{23}$$

$$F_K(n_c) = \exp\left(\int_{-(D+\mu_0)}^{D-\mu_0} \frac{d\omega}{|\omega|}\frac{\rho_A^0(\mu_0+\omega)-\rho_A^0(\mu_0)}{2\rho_A^0(\mu_0)}\right), \tag{24}$$

where D is the half-bandwidth of the noninteracting local DOS $\rho_A^0(\omega)$.

IV. DYNAMICAL MEAN-FIELD THEORY EQUATIONS

The matrix form of the CPA introduced in Refs. 13 and 14 was generalized to the KAM (1) after an appropriate mean-field approximation was made for the Kondo interaction. It allowed for keeping the dynamical aspects of the A sites with their attached spins by means of introducing an additional f-like band of excitations. It supplemented the two bands resulting from the conduction electrons of the A and B sites. In the following we develop for the KAM a matrix-DMFT computational scheme which can be formulated without a mean-field approximation for the Kondo interaction. Note that our approach is different from the dynamical cluster approximation introduced in Ref. 28 since the latter concerns diagonal disorder only.

In the $z\to\infty$ limit for which the following DMFT procedure becomes exact, the system is characterized by only two types of nonequivalent sites (A or B). This is a consequence of the discrete distribution of disorder. Note that the distribution of Kondo temperature or Anderson localization effects discussed in Refs. 5–8 concern models with a continuous distribution of disorder.

A. Dynamical mean-field theory matrix formalism for a binary alloy

The Kondo-alloy Hamiltonian equation (1) can be written as

$$H = \sum_{ij\sigma}\gamma_{ij}\mathbf{P}_i^\dagger\mathbf{W}\mathbf{P}_j c_{i\sigma}^\dagger c_{j\sigma} + \frac{J_K}{2}\sum_i \hat{x}_i \sum_{\sigma\sigma'} S_i^{\sigma\sigma'} c_{i\sigma'}^\dagger c_{i\sigma}, \tag{25}$$

where we introduced the transfer matrix

$$\mathbf{W} = \begin{pmatrix} t_A & t_{AB} \\ t_{AB} & t_B \end{pmatrix}, \tag{26}$$

and the projection operators

$$\mathbf{P}_i = \begin{pmatrix} \hat{x}_i \\ \hat{y}_i \end{pmatrix}, \tag{27}$$

with their conjugates

$$\mathbf{P}_i^\dagger = (\hat{x}_i, \hat{y}_i), \tag{28}$$

where $\hat{x}_i \equiv 1-\hat{y}_i$ is unity if i is an A site and zero otherwise. Here, we have implicitly mapped the initial KAM (1), characterized by a single disordered conduction band, into a two-band effective model. Thereby each site of the underlying periodic lattice acts like being occupied simultaneously by atoms of A and B type. As before, the initial physical Hilbert space corresponding to a single kind of atom per site is recovered by introducing projection operators. They guarantee that a site acts either as an A or B atom. Here, we follow the DMFT formalism,[15,16] which is exact in the limit of a large coordination number z. Considering that the energy of the system is an extensive quantity, this limit requires a rescaling of the hopping energies $t_{ij}=\gamma_{ij}\mathbf{P}_i^\dagger\mathbf{W}\mathbf{P}_j=\tilde{t}_{ij}/\sqrt{z}$, where $\tilde{t}_{ij}$ remains finite (i.e., independent of z) when $z\to\infty$. From the lattice Hamiltonian equation (25) we obtain a local effective action for site 0

$$\mathcal{S}(\hat{x}_0) = -\sum_\sigma \int_0^\beta d\tau \int_0^\beta d\tau' c_{0\sigma}^\dagger(\tau)\mathbf{P}_0^\dagger\mathbf{K}(\tau-\tau')\mathbf{P}_0 c_{0\sigma}(\tau') - \hat{x}_0\frac{J_K}{2}\sum_{\sigma\sigma'}\int_0^\beta d\tau S^{\sigma\sigma'}(\tau)c_{0\sigma}^\dagger(\tau)c_{0\sigma'}(\tau). \tag{29}$$

Here, the kernel $\mathbf{K}$ is a 2×2 matrix, which is a dynamical generalization of the Weiss field usually introduced for a static mean-field approximation. The projection operators $\mathbf{P}_0$ and $\mathbf{P}_0^\dagger$ select the diagonal matrix element $\mathcal{K}_A$ ($\mathcal{K}_B$) of $\mathbf{K}$ depending on whether site 0 is occupied by an A or B atom. The resulting local effective action $\mathcal{S}(\hat{x}_0)$ remains a scalar quantity, which can have two values, i.e., $\mathcal{S}(\hat{x}_0=1)=\mathcal{S}_A$ and $\mathcal{S}(\hat{x}_0=0)=\mathcal{S}_B$. This is a key quantity in the DMFT procedure. It provides a relevant simplification since the local electronic and magnetic Green's functions characterizing the lattice Hamiltonian (25) can now be computed from $\mathcal{S}(\hat{x}_0)$, which invokes local degrees of freedom only. Next, we determine the self-consistent relations allowing us to express the kernel $\mathbf{K}$ as a function of the local Green's functions. Following the standard DMFT formalism, we find

$$\mathbf{K}(i\omega) = (i\omega+\mu)\mathbf{I} - \sum_{ij}\gamma_{0i}\gamma_{j0}\mathbf{W}[\mathbf{P}_i\mathbf{P}_j^\dagger G_{ij}^{(0)}(i\omega)]\mathbf{W}. \tag{30}$$

Here $G_{ij}^{(0)}$ is the cavity Green's function, corresponding to the lattice Hamiltonian (25), but with site 0 excluded. In order to establish a self-consistent relation for the kernel, we perform an infinite order perturbation expansion of Green's functions in terms of the hopping elements $\gamma_{ij}\mathbf{P}_i^\dagger\mathbf{W}\mathbf{P}_j$. Following the DMFT scheme,[15,16] the Green's function G_{ij} for a given distribution of sites A and B is expressed as a sum of all possible paths $i\to i_1\to i_2\cdots i_p\to j$ connecting site i to site j through the sequence of structure factors $\gamma_{i_1 i_2}$. In the limit of large z we may exclude returning paths since their contribu-

tion is of order $1/z^{n+1}$ when n is the number of returns. Thus, each path is factorized in terms of local dressed irreducible *scalar* propagators Π_{ii} which contain information about the local interactions as follows:

$$G_{ij} = \sum_{\text{paths}} \Pi_{ii}\gamma_{ii_1}\mathbf{P}_i^\dagger \mathbf{W}\mathbf{P}_{i_1}\Pi_{i_1i_1}\gamma_{i_1i_2}\mathbf{P}_{i_1}^\dagger \mathbf{W}\mathbf{P}_{i_2}\Pi_{i_2i_2} \cdots \Pi_{i_pi_p}\gamma_{i_pj}\mathbf{P}_{i_p}^\dagger \mathbf{W}\mathbf{P}_j\Pi_{jj}. \tag{31}$$

For the sake of simplicity we have dropped the explicit time dependencies. We will show below that, after averaging over the randomness, these local propagators can be related to a local self-energy. The large-z expansion equation (31) is a *scalar* relation, similar to the one obtained in the usual DMFT approach. The only difference arises from the scalar hopping elements $t_{ij}=\mathbf{P}_i^\dagger \mathbf{W}\mathbf{P}_j\gamma_{ij}$, which here are random. In the following we cast this relation into a 2×2 matrix form, with a periodic effective hopping matrix $\mathbf{W}\gamma_{ij}$ between nearest neighbors. We define

$$\mathbf{G}_{ij} \equiv \mathbf{P}_i G_{ij}\mathbf{P}_j^\dagger = \begin{pmatrix} \hat{x}_i\hat{x}_j G_{ij} & \hat{x}_i\hat{y}_j G_{ij} \\ \hat{y}_i\hat{x}_j G_{ij} & \hat{y}_i\hat{y}_j G_{ij} \end{pmatrix} \tag{32}$$

and

$$\mathbf{\Pi}_{ii} \equiv \mathbf{P}_i \Pi_{ii}\mathbf{P}_i^\dagger = \begin{pmatrix} \hat{x}_i^2\Pi_{ii} & \hat{x}_i\hat{y}_i\Pi_{ii} \\ \hat{y}_i\hat{x}_i\Pi_{ii} & \hat{y}_i^2\Pi_{ii} \end{pmatrix}. \tag{33}$$

Like in Ref. 14, we set $\hat{x}_i=\delta$ (site A) or $1-\delta$ (site B) and later take the limit $\delta\to 0$. The large-z expansion for the Green's function matrix $\mathbf{G}_{ij}$ is obtained by multiplying Eq. (31) with the projection operators $\mathbf{P}_i$ (from the left) and $\mathbf{P}_j^\dagger$ (from the right). After averaging with respect to the different configurations of A and B sites, we find

$$[\mathbf{G}_{ij}] = \sum_{\text{paths}} [\mathbf{\Pi}_{ii}\gamma_{ii_1}\mathbf{W}\mathbf{\Pi}_{i_1i_1}\gamma_{i_1i_2}\mathbf{W}\mathbf{\Pi}_{i_2i_2}\cdots\mathbf{\Pi}_{i_pi_p}\gamma_{i_pj}\mathbf{W}\mathbf{\Pi}_{jj}]. \tag{34}$$

In the large-z limit, we consider only direct paths connecting sites i and j. We assume that a given site i is occupied statistically by an A or a B atom, i.e., is independent of its environment. Therefore, in Eq. (34), each irreducible propagator matrix $\mathbf{\Pi}_{ii}$ can thus be averaged separately, and we find

$$[\mathbf{G}_{ij}] = \sum_{\text{paths}} \mathbf{\Pi}_0\gamma_{ii_1}\mathbf{W}\mathbf{\Pi}_0\gamma_{i_1i_2}\mathbf{W}\mathbf{\Pi}_0\cdots\mathbf{\Pi}_0\gamma_{i_pj}\mathbf{W}\mathbf{\Pi}_0, \tag{35}$$

where $\mathbf{\Pi}_0\equiv[\mathbf{\Pi}_{ii}]$. The matrix relation Eq. (35) between the average Green's functions, the averaged local dressed propagator, and the hopping elements are formally identical to a scalar expansion obtained for a regular periodic system within the standard DMFT formalism.[15,16] We introduce the local Green's function matrix

$$\mathbf{G}_{\text{loc}} \equiv [\mathbf{G}_{ii}] = \begin{pmatrix} xG_A & 0 \\ 0 & (1-x)G_B \end{pmatrix}. \tag{36}$$

Here G_A and G_B are the local Green's functions of an A and a B site, after an average over all the atomic configurations of the surroundings has been taken. Using Eq. (35), the relation between the cavity and full Green's function reads

$$[\mathbf{P}_i\mathbf{P}_j^\dagger G_{ij}^{(0)}] = [\mathbf{G}_{ij}] - [\mathbf{G}_{i0}]\mathbf{G}_{\text{loc}}^{-1}[\mathbf{G}_{0j}]. \tag{37}$$

Averaging over a random distribution of sites A and B restores the translation symmetry of the underlying lattice. The averaged Green's function matrices are thus periodic in space, and we can define their Fourier transforms as

$$\mathbf{G}_{\mathbf{k}} \equiv \sum_{ij} e^{-i\mathbf{k}\cdot(\mathbf{R}_i-\mathbf{R}_j)}[\mathbf{G}_{ij}]. \tag{38}$$

From Eq. (35), we find that the Green's functions are characterized by a local 2×2 self-energy matrix $\mathbf{\Sigma}$

$$\mathbf{G}_{\mathbf{k}}^{-1}(i\omega) = (i\omega+\mu)\mathbf{I} - \mathbf{\Sigma}(i\omega) - \mathbf{W}\gamma_{\mathbf{k}}, \tag{39}$$

where $\mathbf{\Sigma}$ is related to the averaged local propagator by the matrix identity $\mathbf{\Pi}_0^{-1}(i\omega)=(i\omega+\mu)\mathbf{I}-\mathbf{\Sigma}(i\omega)$. The matrix elements of $\mathbf{\Sigma}$ can be expressed in terms of the local average Green's function matrix $\mathbf{G}_{\text{loc}}$ by taking the inverse of

$$\mathbf{G}_{\text{loc}}(i\omega) = \sum_{\mathbf{k}} \mathbf{G}_{\mathbf{k}}(i\omega). \tag{40}$$

Finally, using the relation (37) for the cavity Green's function, together with the expression (30) for the kernel, we find

$$\mathbf{K}(i\omega) = \mathbf{\Sigma}(i\omega) + \mathbf{G}_{\text{loc}}^{-1}(i\omega). \tag{41}$$

Equations (39)–(41) provide a self-consistent relation between the matrix kernel $\mathbf{K}$ and the averaged local Green's function matrix $\mathbf{G}_{\text{loc}}$ as follows:

$$\mathbf{G}_{\text{loc}}(i\omega) = \sum_{\mathbf{k}} [(i\omega+\mu)\mathbf{I} - \mathbf{K}(i\omega) + \mathbf{G}_{\text{loc}}^{-1}(i\omega) - \mathbf{W}\gamma_{\mathbf{k}}]^{-1}. \tag{42}$$

In turn, the local Green's functions G_A and G_B invoked in the definition (36) of $\mathbf{G}_{\text{loc}}$ can be computed for a given kernel $\mathbf{K}$, by considering the cases $\hat{x}_0=0$ and $\hat{x}_0=1$ in the local effective action equation (29). Since the effective action $\mathcal{S}_B$ on sites B is quadratic in terms of electronic operators, we obtain an explicit expression for G_B as follows:

$$G_B(i\omega) = \mathcal{K}_B^{-1}(i\omega). \tag{43}$$

The local Green's functions G_A is obtained from the local effective action on an A atom as follows:

$$\mathcal{S}_A = -\sum_\sigma \int_0^\beta d\tau \int_0^\beta d\tau' c_{0\sigma}^\dagger(\tau)\mathcal{K}_A(\tau-\tau')c_{0\sigma}(\tau') - \frac{J_K}{2}\sum_{\sigma\sigma'}\int_0^\beta d\tau S^{\sigma\sigma'}(\tau)c_{0\sigma}^\dagger(\tau)c_{0\sigma'}(\tau). \tag{44}$$

Apart from the self-consistent relation (42), which can be treated using analytic (and eventually numerical) simple calculations, the main difficulty consists in computing G_A from the local effective action (44). Even if the initial difficulty of studying a lattice model has been consequently reduced into a single site effective model, this issue remains a many body problem. The Kondo interaction part has to be considered using a numerical scheme or appropriate analytical approximations.

Once a self-consistent solution is obtained for $\mathbf{K}$ and $\mathbf{G}_{\text{loc}}$, the $\mathbf{k}$-dependent correlation functions for the conduction

electrons can be obtained using Eqs. (39) and (41). Here, we describe the system with two bands of conduction electrons A and B, whose correlations are characterized by the 2×2 matrix $\mathbf{G_k}$. Invoking the identity $\hat{x}_i\hat{x}_j+\hat{x}_i\hat{y}_j+\hat{y}_i\hat{x}_j+\hat{y}_i\hat{y}_j=\hat{1}$, the physical single band average Green's functions $[G_{ij}]$ can be obtained by adding the four matrix elements of $[\mathbf{G}_{ij}]$. As a consequence, the $\mathbf{k}$-dependent average correlation function for the physical single band of conduction electrons is also obtained by adding the four matrix elements of $\mathbf{G_k}$.

B. Equivalence of the coherent potential approximation and the dynamical mean-field theory

The equivalence of the dynamical CPA and the DMFT was previously proven by Kakehashi on general grounds.[29] As discussed before by applying a 3×3 matrix-CPA approach we were able to describe the important dynamical aspects of the spins of the A sites. Therefore it is reassuring that we can demonstrate the equivalence of the 3×3 matrix-CPA approach with corresponding DMFT equations, when we integrate over the f-electron degrees of freedom in the CPA approach and make a mean-field approximation within the DMFT approach.

1. Expression of the coherent potential approximation equations using a 2×2 matrix formalism

For a demonstration of the equivalence of the two methods we start from a modified version of Eqs. (16)–(19). It is easy to show that after some algebraic modifications the following relations can be derived from these equations:

$$G_A^{ff}(i\omega)=\frac{1}{i\omega+\lambda}+\frac{r^2}{(i\omega+\lambda)^2}G_A^{cc}(i\omega), \tag{45}$$

$$G_A^{fc}(i\omega)=\frac{-r}{i\omega+\lambda}G_A^{cc}(i\omega). \tag{46}$$

The self-consistent CPA equations (16)–(19) can be cast into the form

$$xG_A^{cc}(i\omega)=\sum_{\mathbf{k}}\frac{1}{\Delta_{\mathbf{k}}(i\omega)}[i\omega+\mu-\Sigma_B^{\mathrm{CPA}}(i\omega)-t_B\gamma_{\mathbf{k}}], \tag{47}$$

$$(1-x)G_B^{cc}(i\omega)=\sum_{\mathbf{k}}\frac{1}{\Delta_{\mathbf{k}}(i\omega)}[i\omega+\mu-\Sigma_K(i\omega)-\Sigma_A^{\mathrm{CPA}}(i\omega)-t_A\gamma_{\mathbf{k}}], \tag{48}$$

where

$$\Delta_{\mathbf{k}}(i\omega)=[i\omega+\mu-\Sigma_K(i\omega)-\Sigma_A^{\mathrm{CPA}}(i\omega)-t_A\gamma_{\mathbf{k}}][i\omega+\mu-\Sigma_B^{\mathrm{CPA}}(i\omega)-t_B\gamma_{\mathbf{k}}]-[-\sigma_2(i\omega)-t_{AB}\gamma_{\mathbf{k}}]^2, \tag{49}$$

$$\sigma_2(i\omega)=-t_{AB}\frac{1-2x+x[i\omega+\mu-\Sigma_K(i\omega)]G_A(i\omega)-(1-x)(i\omega+\mu)G_B(i\omega)}{xt_AG_A(i\omega)-(1-x)t_BG_B(i\omega)}. \tag{50}$$

Here we have set

$$\Sigma_A^{\mathrm{CPA}}(i\omega)=-\frac{1-x}{x}\frac{1}{G_A^{cc}(i\omega)}, \tag{51}$$

$$\Sigma_B^{\mathrm{CPA}}(i\omega)=-\frac{x}{1-x}\frac{1}{G_B^{cc}(i\omega)}. \tag{52}$$

We have also introduced the definition

$$\Sigma_K(i\omega)\equiv\frac{r^2}{i\omega+\lambda}. \tag{53}$$

A complete resolution of the model is obtained by the following self-consistent scheme:

(i) Calculate G_A^{cc} and G_B^{cc} from Eqs. (47)–(53), as function of the mean-field parameters r, λ, and μ.

(ii) Calculate G_A^{fc} and G_A^{ff} by using Eqs. (45) and (46).

(iii) Optimize the parameters r, λ, and μ so as to satisfy the mean-field equations (7)–(9).

2. Dynamical mean-field theory and mean-field approximation for the Kondo term

A complete resolution of the matrix-DMFT self-consistent relations requires an impurity solver, in order to compute the local electronic Green's functions G_A related to the local effective action $\mathcal{S}_A$ given by Eq. (44). In order to demonstrate the formal equivalence between the matrix-DMFT and the matrix-CPA approaches, we use the mean-field approximation for the impurity solver. Before, we define the local self-energy due to the Kondo interaction on sites A as follows:

$$\Sigma_K(i\omega)\equiv\mathcal{K}_A(i\omega)-G_A^{-1}(i\omega). \tag{54}$$

Since there is no local interaction on sites B, we have $G_B(i\omega)=\mathcal{K}_B^{-1}(i\omega)$. The relation (41) can be expressed as

$$\mathbf{\Sigma}(i\omega)=\begin{pmatrix}\Sigma_K(i\omega)+\Sigma_A^{\mathrm{CPA}}(i\omega) & \mathcal{K}_{AB}(i\omega)\\ \mathcal{K}_{AB}(i\omega) & \Sigma_B^{\mathrm{CPA}}(i\omega)\end{pmatrix}, \tag{55}$$

with

$$\Sigma_A^{\mathrm{CPA}}(i\omega)=[(1-x)/x]G_A^{-1}(i\omega), \tag{56}$$

$$\Sigma_B^{\mathrm{CPA}}(i\omega) = [x/(1-x)]G_B^{-1}(i\omega). \quad (57)$$

These expressions are identical to Eqs. (51) and (52) obtained within the matrix-CPA approach. Here, as within the CPA approach, the off-diagonal self-energy $\mathcal{K}_{AB}$ (denoted before σ_2) is determined by requiring the vanishing of the off-diagonal elements of $\mathbf{G}_{\mathrm{loc}}$ in Eq. (36). In analogy to Eq. (21), we find

$$\mathcal{K}_{AB}(i\omega) = \sigma_2(i\omega) = -t_{AB}\frac{1-2x+x[i\omega+\mu-\Sigma_K(i\omega)]G_A(i\omega)-(1-x)(i\omega+\mu)G_B(i\omega)}{xt_AG_A(i\omega)-(1-x)t_BG_B(i\omega)}. \quad (58)$$

Combining Eq. (55) with the self-consistent relations Eqs. (36), (39), and (40) we find

$$xG_A(i\omega) = \sum_{\mathbf{k}} \frac{1}{\Delta_{\mathbf{k}}(i\omega)}[i\omega+\mu-\Sigma_B^{\mathrm{CPA}}(i\omega)-t_B\gamma_{\mathbf{k}}], \quad (59)$$

$$(1-x)G_B(i\omega) = \sum_{\mathbf{k}} \frac{1}{\Delta_{\mathbf{k}}(i\omega)}[i\omega+\mu-\Sigma_K(i\omega) - \Sigma_A^{\mathrm{CPA}}(i\omega)-t_A\gamma_{\mathbf{k}}], \quad (60)$$

with

$$\Delta_{\mathbf{k}}(i\omega) = [i\omega+\mu-\Sigma_K(i\omega)-\Sigma_A^{\mathrm{CPA}}(i\omega)-t_A\gamma_{\mathbf{k}}][i\omega+\mu - \Sigma_B^{\mathrm{CPA}}(i\omega)-t_B\gamma_{\mathbf{k}}]-[-\sigma_2(i\omega)-t_{AB}\gamma_{\mathbf{k}}]^2, \quad (61)$$

which are formally equivalent to the relations Eqs. (47)–(49) obtained from the matrix form of the CPA approach.

The matrix-DMFT approach developed here is performed without any approximation concerning the local Kondo interaction. An impurity solver is required in order to calculate the local Green's functions from the local effective action $\mathcal{S}_A$ defined in Eq. (44), and then to compute the Kondo self-energy Σ_K. For example, the mean-field approximation can be performed as described in the previous section (CPA), leading to the same set of saddle point relations as Eqs. (7)–(9). This method, developed in the framework of a Kondo-alloy model, can be generalized to other alloy models with strong local correlations.

C. Bethe lattice with infinite coordination

The DMFT formalism described in the previous section is exact in the limit of an infinite coordination number z. It can be applied to any underlying periodic lattice, which is defined by its structure factor $\gamma_{\mathbf{k}}$. In order to study the Kondo-alloy model defined by the Hamiltonian equation (1) numerically, it is convenient to consider a Bethe lattice. For a similar approach applied to ferromagnetic semiconductors, see Ref. 30. In this specific case, the self-consistent equations are much simpler, and the general physical properties of the system are preserved. The main argument is that the density of states (DOS) for a Bethe lattice without disorder and without Kondo impurities is of a semielliptic form. Since most of the electronic properties depend on the DOS they should be robust with respect to a Bethe lattice.

Applying the DMFT formalism described in the previous section to a Bethe lattice, we obtain a local effective action for the two kinds of sites

$$\mathcal{S}_A = -\sum_{\sigma}\int_0^{\beta}d\tau\int_0^{\beta}d\tau' c_{A\sigma}^{\dagger}(\tau)\mathcal{K}_A(\tau-\tau')c_{A\sigma}(\tau') - \frac{J_K}{2}\sum_{\sigma\sigma'}\int_0^{\beta}d\tau S^{\sigma\sigma'}(\tau)c_{A\sigma}^{\dagger}(\tau)c_{A\sigma'}(\tau), \quad (62)$$

$$\mathcal{S}_B = -\sum_{\sigma}\int_0^{\beta}d\tau\int_0^{\beta}d\tau' c_{B\sigma}^{\dagger}(\tau)\mathcal{K}_B(\tau-\tau')c_{B\sigma}(\tau'). \quad (63)$$

They are formally equivalent to the compact expression equation (29). The main simplification obtained by considering a Bethe lattice rests on the fact that the cavity Green's functions involved in Eq. (30) can now be replaced by local full Green's functions. This procedure is exact in the limit of a large coordination number z. The Bethe lattice self-consistent relations for the kernels $\mathcal{K}_A$ and $\mathcal{K}_B$ are thus

$$\mathcal{K}_A(i\omega) = i\omega+\mu-x\tilde{t}_A^2G_A^{cc}(i\omega)-(1-x)\tilde{t}_{AB}^2G_B^{cc}(i\omega), \quad (64)$$

$$\mathcal{K}_B(i\omega) = i\omega+\mu-x\tilde{t}_{AB}^2G_A^{cc}(i\omega)-(1-x)\tilde{t}_B^2G_B^{cc}(i\omega), \quad (65)$$

where, in the large-z limit, the nearest-neighbor hoppings have been rescaled: $t_A \equiv \tilde{t}_A/\sqrt{z}$, with similar definitions for $\tilde{t}_B$ and $\tilde{t}_{AB}$. We then apply the mean-field approximation, described in the first section, as an impurity solver for the local effective action $\mathcal{S}_A$ of an A site. Within the mean-field approximation, the effective action equations (62) and (63) are quadratic and the local Green's functions can in turn be expressed explicitly as functions of the kernels $\mathcal{K}_A$ and $\mathcal{K}_B$

$$\begin{pmatrix} G_A^{ff}(i\omega) & G_A^{fc}(i\omega) \\ G_A^{cf}(i\omega) & G_A^{cc}(i\omega) \end{pmatrix} = \begin{pmatrix} i\omega+\lambda & r \\ r & \mathcal{K}_A(i\omega) \end{pmatrix}^{-1}, \quad (66)$$

$$G_B^{cc}(i\omega) = \mathcal{K}_B^{-1}(i\omega). \quad (67)$$

Together with Eqs. (64) and (65) and with the mean-field equations (7)–(9) we have a complete set of self-consistent relations for the local Green's functions and the effective parameters r, λ, and μ.

For a given set of parameters x, n_c, J_K, t_A, t_B, and t_{AB} and the temperature $T=1/\beta$, we compute the effective param-

eters r, λ, and μ. The latter are determined by solving the mean-field equations (7)–(9), after they have been rewritten in term of Matsubara frequencies. These three equations for r, λ, and μ are solved numerically using the Newton-Raphson method.

1. Calculation of the Green's functions

Here, we consider an estimate of r, λ, and μ, and we determine numerically the Green's functions for a given Matsubara frequency $i\omega_n$. We exclude the trivial cases $x=0$ and $x=1$ for which the Green's functions can be expressed analytically. Invoking Eqs. (64)–(67), we find self-consistent relations for $G_A^{cc}(i\omega_n)$ and $G_B^{cc}(i\omega_n)$ as follow:

$$G_A^{cc}(i\omega_n) = \frac{1}{\tilde{t}_A\sqrt{x}}\mathcal{G}_0\left[\frac{\Omega_A(i\omega_n)}{\tilde{t}_A\sqrt{x}}\right], \tag{68}$$

$$G_B^{cc}(i\omega_n) = \frac{1}{\tilde{t}_B\sqrt{1-x}}\mathcal{G}_0\left[\frac{\Omega_B(i\omega_n)}{\tilde{t}_B\sqrt{1-x}}\right], \tag{69}$$

where $\Omega_A(i\omega_n) \equiv i\omega_n + \mu - r^2/(i\omega_n + \lambda) - (1-x)\tilde{t}_{AB}^2 G_B^{cc}(i\omega_n)$ and $\Omega_B(i\omega_n) \equiv i\omega_n + \mu - x\tilde{t}_{AB}^2 G_A^{cc}(i\omega_n)$. The dimensionless function $\mathcal{G}_0[\Omega] \equiv \frac{\Omega}{2}[1-\sqrt{1-4/\Omega^2}]$ is characteristic of a Bethe lattice structure. Equations (68) and (69) are solved numerically using a standard iterative algorithm. Once $G_A^{cc}(i\omega_n)$ and $G_B^{cc}(i\omega_n)$ are computed, $G_A^{fc}(i\omega_n)$ and $G_A^{ff}(i\omega_n)$ are obtained using Eqs. (64) and (66).

2. Numerical determination of the Kondo temperature

We define the Kondo temperature T_K as the temperature at which the effective hybridization r vanishes. An analytical relation between T_K and the local electronic DOS without Kondo interaction is provided by Eq. (22). Here, we determine T_K numerically for a given set of parameters x, n_c, J_K, t_A, t_B, and t_{AB}. First, we compute the parameter r using the Newton-Raphson method and for different temperatures. Then, we identify T_K as the temperature for which r continuously vanishes. The numerical error can be controlled by the temperature steps, which we took to be approximately of the order of 1%.

3. Numerical determination of the local static magnetic susceptibility

The local static magnetic susceptibility on a magnetic site is defined as

$$\chi_{\text{loc}}(T) \equiv \frac{1}{3}\int_0^{1/T} d\tau \langle \mathbf{S}(\tau)\cdot\mathbf{S}(0)\rangle, \tag{70}$$

where the dynamical spin-spin correlation function is computed from the local effective action on a magnetic site [i.e., from the action defined by Eq. (62)]. In the mean-field approximation, the dynamical spin-spin correlation function can be expressed as

$$\frac{1}{3}\langle \mathbf{S}(\tau)\cdot\mathbf{S}(0)\rangle = G_A^{ff}(\tau)G_A^{ff}(-\tau). \tag{71}$$

Using Eqs. (70) and (71), $\chi_{\text{loc}}(T) = T\Sigma_{n=-\infty}^{+\infty}[G_A^{ff}(i\omega_n)]^2$ is computed numerically. The low temperature behavior is characterized by the energy scale

$$T_0 \equiv 1/4\chi_{\text{loc}}(T=0). \tag{72}$$

We estimate T_0 by computing $\chi_{\text{loc}}(T)$ for T much lower than the Kondo temperature obtained with the same set of parameters.

4. Numerical determination of the local density of states

We define the local density of electronic states (DOS) associated with G_A^{cc} and G_B^{cc}

$$\rho_{A/B}(\omega) \equiv -(1/\pi)\text{Im}\, G_{A/B}^{cc}(\omega + i0^+), \tag{73}$$

and the averaged local DOS

$$\rho(\omega) = x\rho_A(\omega) + (1-x)\rho_B(\omega). \tag{74}$$

Here, within CPA or DMFT, all the local DOS's of A sites are the same while a more accurate treatment would show a spread. This can be obtained by randomizing the distribution of the hopping matrix elements t_A, t_B, and t_{AB}. This could be done within the present DMFT formalism. By construction ρ_A, ρ_B, and ρ have each a total spectral weight of unity, and A (B) atoms contribute with a weight x $(1-x)$ to the averaged DOS ρ. We determine $\rho_A(\omega)$ and $\rho_B(\omega)$ numerically for a given set of parameters x, n_c, J_K, t_A, t_B, and t_{AB} and a temperature T. First, we compute the parameters r, λ, and μ using the Newton-Raphson method. Then we compute $G_{A/B}^{cc}(\omega + i\epsilon)$, where ω is a real number and ϵ is a small positive constant number. This computation is done by solving Eqs. (68) and (69) numerically, after having replaced $i\omega_n$ by $\omega + i\epsilon$.

V. APPLICATIONS OF THE FORMALISM

A. Off-diagonal randomness: Nonmagnetic random alloy

1. Formalism

In this section we consider off-diagonal randomness, i.e., hopping matrix elements. The model is defined by the Hamiltonian equation (1) without the Kondo interaction. This is a standard situation for the CPA and we discuss this case here only because we want to combine it later with the Kondo problem. We know that the CPA misses certain localization effects. Their importance in connection with Kondo effect has been discussed in Ref. 12. Since the spin components are decoupled, the system corresponds to a random tight-binding model of conduction electrons, identical to the one considered in Refs. 13 and 14. Thus $G_{ij}(\tau-\tau') \equiv -\langle T_\tau c_i(\tau)c_j^\dagger(\tau')\rangle$ is the electron Green's function defined for imaginary time. Since here we do not consider the Kondo interaction, the self-consistent equation for the averaged Green's function can equivalently be obtained either from the matrix form of the CPA approach [Eqs. (47)–(49), (51), and (52)] or from the matrix-DMFT approach [Eqs. (56),

(57), (59), and (61)]. In both cases the Kondo self-energy $\Sigma_K=0$. We find

$$xG_A(i\omega)=\sum_{\mathbf{k}}\frac{1}{\Delta_{\mathbf{k}}(i\omega)}[i\omega-\Sigma_B^{\mathrm{CPA}}(i\omega)-t_B\gamma_{\mathbf{k}}], \quad (75)$$

$$(1-x)G_B(i\omega)=\sum_{\mathbf{k}}\frac{1}{\Delta_{\mathbf{k}}(i\omega)}[i\omega-\Sigma_A^{\mathrm{CPA}}(i\omega)-t_A\gamma_{\mathbf{k}}], \quad (76)$$

$$\Delta_{\mathbf{k}}(i\omega)=[i\omega-\Sigma_A^{\mathrm{CPA}}(i\omega)-t_A\gamma_{\mathbf{k}}][i\omega-\Sigma_B^{\mathrm{CPA}}(i\omega)-t_B\gamma_{\mathbf{k}}]-[-\sigma_2(i\omega)-t_{AB}\gamma_{\mathbf{k}}]^2, \quad (77)$$

$$\Sigma_A^{\mathrm{CPA}}(i\omega)=[(1-x)/x]G_A^{-1}(i\omega), \quad (78)$$

$$\Sigma_B^{\mathrm{CPA}}(i\omega)=[x/(1-x)]G_B^{-1}(i\omega), \quad (79)$$

$$\sigma_2(i\omega)=-t_{AB}\frac{1-2x+i\omega[xG_A(i\omega)-(1-x)G_B(i\omega)]}{xt_AG_A(i\omega)-(1-x)t_BG_B(i\omega)}. \quad (80)$$

Here G_A and G_B are the local Green's functions G_{ii} on a site i of kind A (or B), obtained by averaging over all the other site configurations A or B. For the sake of simplicity, we drop the chemical potential μ. This convention implies that the Fermi level energy is zero when the electron band is half-filled.

We did not find a general analytic solution for this set of equations, so that a numerical evaluation is required. Nevertheless, a dimensionless ratio emerges from these expressions

$$\alpha=t_{AB}/\sqrt{t_At_B}, \quad (81)$$

which compares the energy characterizing the hopping of electrons between sites A and B with the hopping energies within an A and a B sublattice. Intuitively, if $\alpha>1$, the electronic levels of lowest energy will be dominated by hopping between A-B neighboring sites. In the opposite case of $\alpha<1$, hopping within pure A or pure B sublattices dominates.

2. Numerical results: Local density of states

Choosing a Bethe tree structure as underlying lattice (this corresponds to a semielliptic DOS for the pure A or pure B system), we have computed $\rho_A(\omega)$ and $\rho_B(\omega)$ numerically for different values of the hopping elements. For the purpose of simplification, we present here some numerical results obtained for $t_A=t_B\equiv t$ only. In the following, all energies are expressed in units of $\tilde{t}\equiv t\sqrt{z}$, where z is the coordination number of the lattice, and different values of $\alpha=t_{AB}/t$ are considered.

Figure 1 depicts the effect of off-diagonal randomness on the local DOS's ρ_A, ρ_B, and ρ. The plots presented here are obtained for a concentration $x=20\%$ of atoms of kind A. Qualitatively similar behavior is found for different concentrations. For $\alpha=1$ ($t_{AB}=t_A=t_B$), our numerical results recover the semielliptic DOS corresponding to a regular tight-binding model. In the regime $\alpha<1$, the DOS remains semielliptic-like, with a rescaled bandwidth [see also Fig. 3(b)]. In the regime $\alpha>1$, the DOS ρ_A corresponding to the minority atoms splits into two satellite peaks, centered around the energy $\pm t_{AB}$, while the DOS ρ_B corresponding to the majority atoms shows both a two satellite peak structure and a coherent peak around $\omega=0$. The latter is reminiscent of the semielliptic one obtained in the absence of disorder ($\alpha=1$). As a consequence, the averaged local DOS ρ is also characterized by a central peak and two satellites.

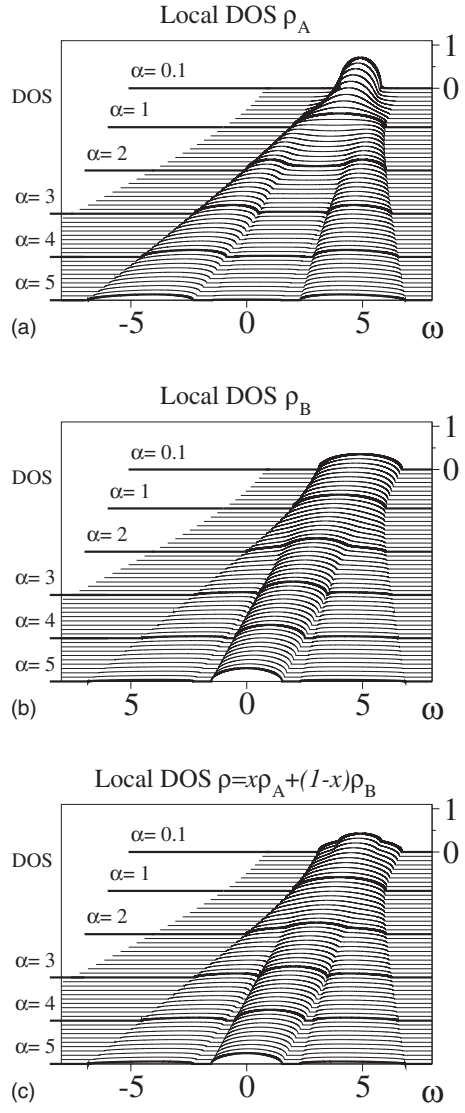

FIG. 1. (a) Local DOS $\rho_A(\omega)$ on a site A. (b) Local DOS $\rho_B(\omega)$ on a site B. (c) Average local DOS $\rho(\omega)=x\rho_A(\omega)+(1-x)\rho_B(\omega)$. The curves correspond to a concentration $x=20\%$. Each plot corresponds to a fixed value of $\alpha=t_{AB}/t$, which varies from 0.1 (top) to 5 (down) in steps of 0.1. The curves have been shifted both vertically and horizontally, with numerical scales written explicitly only for $\alpha=0.1$ (vertical direction) and $\alpha=5$ (horizontal axis). The energy is in units of $\tilde{t}=t_A\sqrt{z}=t_B\sqrt{z}$.

Regime $\alpha>1$. Integrating the local DOS, we define the average densities of electrons on sites A and B in the Fermi sea, as function of the Fermi energy E_F

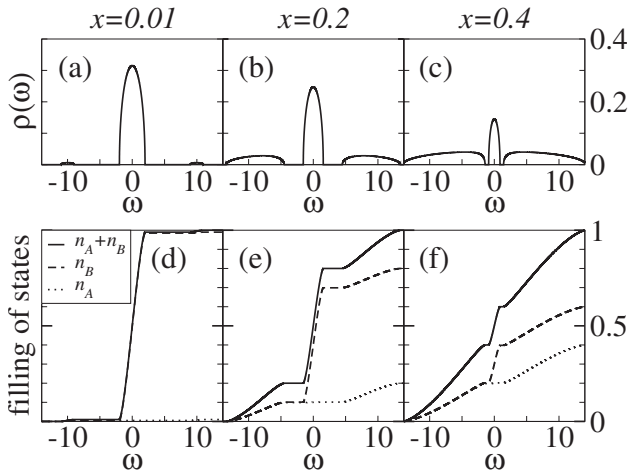

FIG. 2. [(a)–(c)] Average local DOS $\rho(\omega)=x\rho_A(\omega)+(1-x)\rho_B(\omega)$ (top). [(d)–(f)] Filling of states on A sites (dotted line), B sites (dashed line), and both A and B sites (solid line), as a function of the Fermi level energy. Numerical results for $\alpha=10$. The energy is in units of $\tilde{t}=t_A\sqrt{z}=t_B\sqrt{z}$. The concentration x of A atoms is equal to 0.01 [(a) and (d)], 0.2 [(b) and (e)], and 0.4 [(c) and (f)]. The curves corresponding to $x=0.6;0.8;0.99$ can be deduced by inverting A and B.

$$n_{A/B} \equiv c_{A/B}\int_{-\infty}^{E_F} d\omega \rho_{A/B}(\omega), \tag{82}$$

where $c_A=x$ and $c_B=1-x$. We analyze in Fig. 2 the microscopical origin of the satellites and central peak in the averaged DOS for large values of α. It appears that the two satellite peaks correspond to electronic excitations which are equally distributed over A and B sites, while the central peak is due to excitations of electrons on the majority B sites. Our interpretation is the following: when $\alpha>1$, the electronic states with the lowest energy are obtained by forming A-B bonds. The deepest levels of the Fermi sea thus correspond to electronic wave functions localized on clusters formed by alternating A and B atoms. In the following, we call the latter "AB clusters." We interpret the two satellite peaks as bonding and antibonding electronic states formed in these AB clusters. In the large-z limit, each A atom can be associated with a neighboring atom B. Choosing the latter to point into the same (arbitrary) "direction" guarantees that the so formed AB clusters contain exactly the same number of A and B atoms. As a consequence, the statistical weight of the AB clusters is $2x$, which is twice the concentration of the minority atoms A. Whether a given B site belongs to an AB cluster or to the embedding surface is left open. Nevertheless, the satellite peaks characterizing the DOS for $\alpha \gg 1$ have precisely the statistical weight $2x$, which is equally distributed over A and B atoms [see Figs. 2 and 3(a)]. The remaining B atoms constitute hypersurfaces embedding the AB clusters. Considering that the dimension of the system is proportional to z, the embedding surfaces provide in the large-z limit a contribution to the DOS (central peak) which is qualitatively similar to the one obtained for $\alpha=1$ (i.e., semielliptic here). The spectral weight of the latter is $1-2x$. Gaps in the local

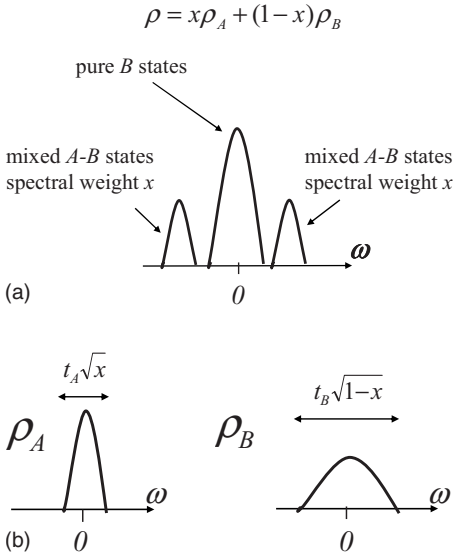

FIG. 3. Schematic plot of (a) the average local density of states of the conduction electrons $\rho=x\rho_A+(1-x)\rho_B$ in the limit $\alpha=t_{AB}/\sqrt{t_A t_B}\gg 1$; (b) the local densities of states of the conduction electrons ρ_A (on a site A) and ρ_B (on a site B) in the limit $\alpha=t_{AB}/\sqrt{t_A t_B}\ll 1$. The concentration of atoms A is assumed to be $x<1/2$.

DOS, with two satellites and a central peak, appear only above a critical value of α. This is seen in Fig. 1.

Regime $\alpha<1$. In the limit $\alpha\to 0$, the two subsystems A and B decouple, and the averaged local DOS's ρ_A and ρ_B can be deduced from the DOS of a pure system by rescaling the energy as $t_A\sqrt{x}$ and $t_B\sqrt{1-x}$, respectively [see Fig. 3(b)]. As a consequence, when $t_A=t_B$, electrons with the lowest energy occupy predominantly majority atoms. When the density of conduction electrons is sufficiently large, the Fermi level moves into a region where electrons occupy both A and B sites. For that reason, the regime $\alpha<1$ is qualitatively not very different from the regime $\alpha=1$, except in the limit of a low density of conduction electrons.

B. Diagonal randomness: Kondo alloy

We consider next the transition between a dilute and a dense Kondo system. The model is defined by the KAM equation (1), with a periodic hopping element for the conduction electrons $t\equiv t_A=t_B=t_{AB}$. The limit $x\to 0$ corresponds to a single impurity Kondo model (SIKM), while $x=1$ describes a Kondo lattice model (KLM). These models have been extensively studied[3] by using various approximations. When we consider a paramagnetic ground state, two energy scales are required[31–33] in order to describe the low temperature physical properties: T_K characterizes the onset of the Kondo effect, and T_{FL} characterizes the low temperature thermodynamics.

On one side, the exact solution of the SIKM, based on the Bethe ansatz,[34,35] proves that these two scales are identical in the dilute limit $x\to 0$. The low temperature physical properties of the SIKM are thus universal (i.e., independent from the lattice structure, electronic filling, and Kondo coupling)

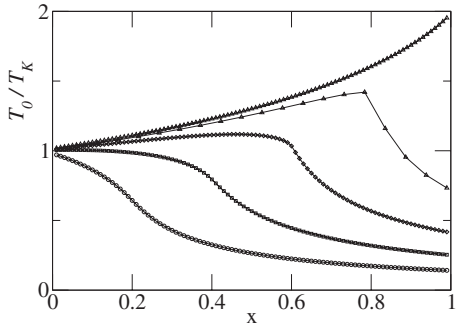

FIG. 4. Ratio between $T_0=1/4\chi_{\rm loc}(T=0)\approx T_{\rm FL}$ and T_K as a function of the Kondo impurity concentration x. The different curves correspond to different electronic filling: from top to bottom, $n_c=1;0.8;0.6;0.4;0.2$. The solid lines are guide for the eyes. The curves have been computed for hopping matrix elements $t\equiv t_A=t_B=t_{AB}$ and $J_K/t\sqrt{z}=1.5$.

as soon as all the energy scales are rescaled by T_K.

On the other side, for the KLM these two energy scales are different. In earlier works it had been suggested that for small conduction electron densities $T_{\rm FL}$ is strongly reduced, i.e., to $T_{\rm FL}\to T_K^2/t$ because of conduction electron "exhaustion" when singlet states form.[36–38] However, this has turned out not to be the case and $T_{\rm FL}$ is of the same order as T_K.[27–38]

The KAM which is studied here allows for describing the crossover between the dilute regime (with $T_{\rm FL}/T_K=1$) and the dense regime (with $T_{\rm FL}/T_K$ depending on the electronic filling). The zero temperature static local magnetic susceptibility of the A sites is $\chi_{\rm loc}(T=0)\equiv\frac{1}{3}\lim_{T\to 0}\int_0^{1/T}d\tau\langle\mathbf{S}(\tau)\cdot\mathbf{S}(0)\rangle$. We define an energy scale $T_0\equiv 1/4\chi_{\rm loc}(T=0)$, which is closely related to $T_{\rm FL}$.[27]

Figure 4 depicts the evolution of the ratio T_0/T_K for different values of the electronic filling n_c. It starts from $T_0/T_K=1$ in the dilute limit $x\to 0$, as expected for the SIKM. With decreasing filling n_c this ratio is lower in the dense limit $x=1$ corresponding to the KLM. This shows clearly that the crossover between the dense and the dilute regimes occurs when the concentration x of Kondo impurities is equal to the electronic filling n_c. Note that similar results have been obtained recently by Kaul and Vojta for a 20×20 site square lattice (compare Fig. 4 with Fig. 2 of Ref. 12).

The above feature can also be observed from the spectral function ρ_A, i.e., the local electronic DOS of a Kondo impurity. This is illustrated in Fig. 5 for an electronic filling of $n_c=0.6$. Above the Kondo temperature, ρ_A has the same semielliptic shape as in the absence of a localized spin. When $T\approx T_K$ a Kondo resonance develops at the Fermi level. Neither the quantitative value of T_K nor the shape of the resonance depend on the concentration x. This suggests that the onset of the Kondo effect at T_K is not a collective coherent effect, but results from incoherent scattering of conduction electrons by the magnetic impurities. When the temperature is decreased far below the Kondo temperature, collective coherent screening takes place, which is accompanied by the onset of the Fermi-liquid regime. For $T\ll T_K$ the local DOS of A sites depends on the concentration and shows in the dilute regime $x\to 0$ the standard Kondo resonance, while a

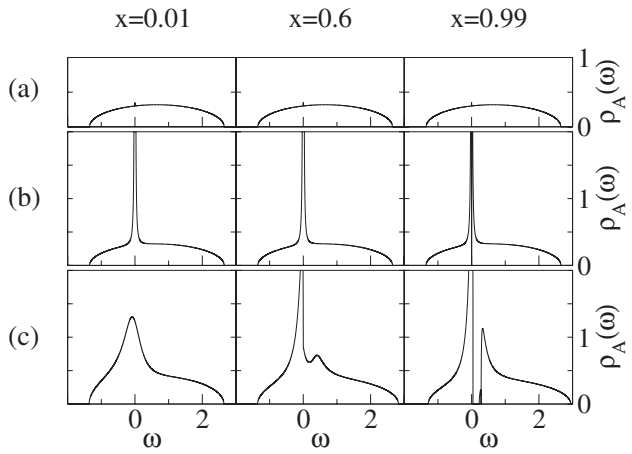

FIG. 5. Local electronic DOS on a magnetic site for an electronic filling $n_c=0.6$. Kondo impurity concentrations $x=0.01$ (diluted), $x=n_c=0.6$ (intermediate), and $x=0.99$ (dense). The energy unit is $\tilde{t}\equiv t_A\sqrt{z}=t_B\sqrt{z}=t_{AB}\sqrt{z}$ and $J_K/\tilde{t}=1.5$. (a) Temperature $T>T_K$. (b) Temperature $T\approx T_K$. (c) Temperature $T=T_K/300$.

gap occurs in the dense regime $x\approx 1$. We are aware that the presence of a Kondo gap is an artifact of the mean-field approximation which we have introduced. Numerical studies of the KLM without this approximation show, however, that a pseudogap will form.[39] Similarly to what we obtained for the ratio T_0/T_K, we find that the crossover between the dilute regime (without gap) and the dense regime (with a gap) occurs for $x=n_c$. Figure 5 depicts this behavior for an electronic filling $n_c=0.6$. Similar results are obtained for $n_c=0.2;0.4;0.8$.

It appears that the crossover between a dilute and a dense Kondo system occurs when the concentration x of Kondo impurities is equal to the electronic filling n_c. We expect this result to apply also to the Anderson model, which still contains the charge degrees of freedom associated with the spins $\mathbf{S}_i$ of the A sites. This explains why the single impurity models, characterized by a unique low temperature scale $T_0=T_K$, are still able to describe the low temperature properties of alloys with a significant concentration of magnetic impurities, here A sites. As a consequence, in the experimental literature, the Kondo temperature of Kondo-like alloys is frequently estimated from different physical quantities, with no distinction being made between the quantities characterizing the Fermi-liquid regime and those characterizing the onset of the Kondo effect. Nevertheless, two different energy scales, $T_{\rm FL}$ and T_K, have been measured experimentally and analyzed for several rare earth alloys. For example, some very promising experimental results dedicated to an analysis of the crossover between diluted and dense impurity systems can be found in Ref. 40 (alloy $Yb_{1-x}Lu_xAl_3$), in Ref. 41 ($Ce_{1-x}La_xIr_2Ge_2$), in Ref. 42 ($CeNiSi_2$), or in Ref. 43 ($Ce_xLa_{1-x}Pb_3$). For instance, in Ref. 43, the resistivity, magnetic susceptibility, and specific heat of the alloy $Ce_xLa_{1-x}Pb_3$ are compared to the prediction of a single-ion Kondo model. It appears that the latter, characterized by a single energy scale $T_0=T_K$, reproduces very well the experimental measurements when $x<0.8$. The onset of interfer-

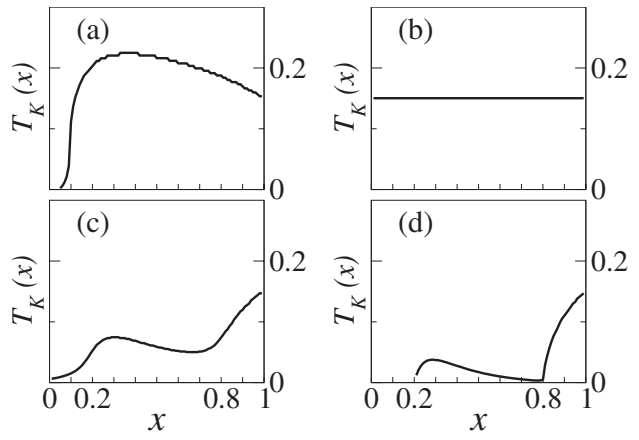

FIG. 6. Kondo temperature T_K as a function of concentration x of A sites. Electronic filling is n_c=0.4. Kondo coupling is J_K=1.5. The energy scale is $\tilde{t} \equiv t_A\sqrt{z}=t_B\sqrt{z}$. (a) α=0. (b) α=1. (c) α=2. (d) α=3.

ence effects between Ce ions is observed only at high concentrations $x>0.8$. Our results predict that the crossover between the dense and diluted regimes corresponds to $x=n_c$. We suggest a more systematic experimental study of such a crossover for Ce-La and Yb-Lu Kondo alloys.

C. Combined effects of randomness

In this section we consider the KAM equation (1) with randomness of the electronic hopping matrix elements t_{ij} and of Kondo alloying effects. We study the effect of alloying described, respectively, by the parameters x and n_c, and of randomness, characterized by the parameter α defined by Eq. (81). For the sake of clarity we discuss here only the behavior of the two low temperature energy scales introduced in the previous section: the Kondo temperature T_K, characterizing the onset of incoherent singlet formation, and T_{FL}, characterizing the onset of a coherent Fermi-liquid state. A good estimate of the latter can be obtained from the static local magnetic susceptibility at T=0 if we approximate T_{FL} by $T_0=1/4\chi_{\mathrm{loc}}(T=0)$.

1. Kondo temperature

Next we study the effect of the concentration x on the Kondo temperature by considering various values of randomness α and electronic filling n_c. The main variations we observe for T_K result from the effects of randomness on the noninteracting local DOS ρ_A, which are analyzed in Sec. V A.

Figure 6 shows the dependence of the Kondo temperature with respect to x. Without randomness (i.e., for α=1), the Kondo temperature does not depend on x [see Fig. 6(b)]. This reflects the fact that T_K characterizes incoherent scattering of the conduction electrons on the spins $\mathbf{S}_i$. Due to the exponential dependence of T_K on $\rho_A(E_F)$ [see Eq. (23)], with possible gap opening (in the regime $\alpha>1$) or bandwidth renormalization (in the regime $\alpha<1$), T_K can be strongly reduced in certain regimes of concentrations x as soon as $\alpha \neq 1$.

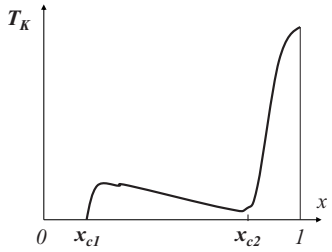

FIG. 7. Schematic plot of the Kondo temperature T_K as a function of concentration x of A sites for strong A-B electronic hopping ($\alpha=t_{AB}/\sqrt{t_A t_B} \gg 1$). Three regimes are recognized, separated by the concentrations x_{c1} and x_{c2}.

Regime $\alpha<1$. A decrease of α does not really change the value of T_K, except in the dilute regime $x \ll 1$, where T_K is strongly reduced [see Fig. 6(a)]. The reason is that when x and α are small, the effective bandwidth of the local electronic DOS on A sites is strongly reduced [see Fig. 3(b)]. Therefore the conduction electrons will fill the states at the nonmagnetic B sites and $\rho_A(E_F)$ is reduced.

Regime $\alpha>1$. When α increases, two critical concentrations x_{c1} and x_{c2} occur. They define three regimes [see Figs. 6(c), 6(d), and 7]. This is a consequence of the complex structure of the local DOS discussed in Sec. V A, with a central and two satellite peaks [see Fig. 3(a)].

For $x>x_{c2}$, the Kondo or A sites are in the majority. The Fermi level is in the central peak of the DOS, which precisely corresponds to electronic excitations on A sites.

When x decreases from 1 to x_{c2}, the DOS is modified such that the Fermi level approaches the band edge of the central peak. As a consequence, T_K decreases and can even vanish for $x=x_{c2}$ if α is large enough.

For $x_{c1}<x<x_{c2}$, the Fermi level is positioned in a satellite peak, corresponding to electronic excitations on both magnetic and nonmagnetic sites. T_K is finite but reduced compared to its value at x=1. For $x<x_{c1}$, the Fermi level is in the central peak, but now the latter corresponds to excitations on the nonmagnetic B sites which here are in the majority. As a consequence, ρ_A and T_K are strongly reduced in this regime and can even vanish if α is large enough. Note that at low x and large α, the numerical accuracy is limited because of the required summation over Matsubara frequencies.

Relations between x_{c1}, x_{c2} and the electronic filling n_c can be obtained in the large α limit from the observation that the spectral weight of the satellite peaks is proportional to the concentration of the minority A or B sites. Figure 3(a) depicts the average local DOS for $\alpha \gg 1$ and without Kondo interaction. The Fermi level is in the central peak if and only if the electronic occupation per spin component $n_c/2$ satisfies the criteria $x<n_c/2<1-x$. We thus find

$$x_{c1}=n_c/2, \tag{83}$$

$$x_{c2}=1-n_c/2. \tag{84}$$

These relations corresponds to the critical values x_{c1}=0.2 and x_{c2}=0.8 obtained numerically for n_c=0.4 [see Figs. 6(c)

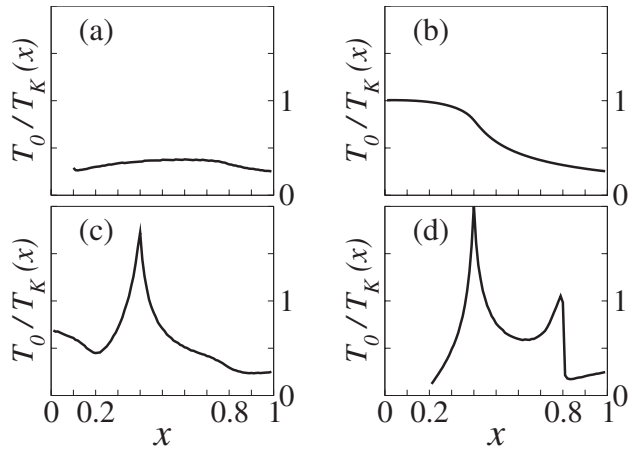

FIG. 8. Ratio of $T_0 \equiv 1/4\chi_{\rm loc}(T=0) \approx T_{\rm FL}$ and the Kondo temperature T_K as a function of the concentration x of A sites. Electronic filling: $n_c=0.4$. Kondo coupling: $J_K=1.5$. The energy scale is $\tilde{t} \equiv t_A\sqrt{z}=t_B\sqrt{z}$. (a) $\alpha=0$. (b) $\alpha=1$. (c) $\alpha=2$. (d) $\alpha=3$.

and 6(d)]. They are also verified by numerical results for other electronic fillings.

2. Kondo versus Fermi-liquid temperature

In the following we discuss the ratio between $T_{\rm FL}$ and T_K. The effect of varying the electronic filling was discussed in Sec. V B for $\alpha=1$. Figure 8(b) reproduces for convenience the plot of T_0/T_K as a function of x corresponding to $\alpha=1$ and $n_c=0.4$ shown in Fig. 4. The other plots of Fig. 8 depict the effect of varying α with the electronic filling kept fixed. We obtained similar results with other values of n_c. For the sake of clarity, we show here only the numerical results which we obtained for $n_c=0.4$.

Regime $\alpha<1$. The crossover separating the dense and dilute regime is well localized at $x=n_c$ and $\alpha=1$, and smoothed when α decreases [compare Figs. 8(a) and 8(b)]. At low concentrations, numerical calculations are less accurate. This is related to the strong decrease of T_K when $x \to 0$ [see Fig. 6(a)]. For this reason, we are not able to provide reasonable results concerning T_0/T_K for $x<0.1$.

Regime $\alpha>1$. When α increases, two different effects occur: the crossover between the dense and dilute regime becomes more pronounced around $x=n_c$ [see Figs. 8(c) and 8(d)] and some "anomalies" occur at the critical concentrations x_{c1} and x_{c2} [see Eq. (84)]. When x is approaching any of these critical values, the ratio T_0/T_K becomes small [see $x=x_{c1}=0.2$ and $x=x_{c2}=0.8$ on Fig. 8(d)]. Similar results were obtained for other values of n_c (0.2; 0.4; 0.6; 0.8). The general shape of the curve T_0/T_K in the regime $\alpha>1$ is depicted in Fig. 9.

When $T_0/T_K \approx 1$, the physical properties of the system are characterized by two universal temperature regimes: for $T>T_K$, the thermodynamic and transport properties are those of a light Fermi liquid (due to the conduction electrons), and the magnetic properties are characteristic of free moments (for example, the magnetic susceptibility follows a Curie law). For $T<T_0$, the physical properties correspond to a heavy Fermi liquid.

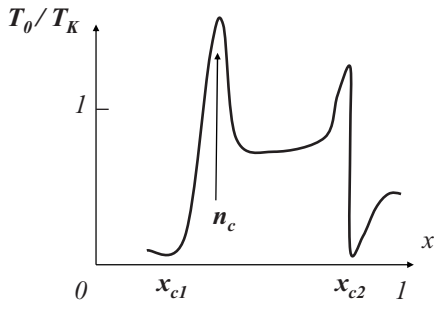

FIG. 9. Schematic plot of the ratio between $T_0 \equiv 1/4\chi_{\rm loc}(T=0) \approx T_{\rm FL}$ and the Kondo temperature T_K as a function of the Kondo impurity concentration x for $\alpha \gg 1$ (i.e., large A-B hopping matrix element).

When $T_0/T_K \ll 1$, an intermediate regime occurs, corresponding to $T_0<T<T_K$, for which the temperature dependence of the physical properties might have non-Fermi-liquid or spin-liquid behavior.

Note that the peak at $x=0.8$ in Fig. 8(d) (and more generally at $x=x_{c2}$ on Fig. 9) has been explained in Ref. 44 to which we refer.

VI. SUMMARY AND CONCLUSIONS

The aim of this investigation has been to develop a description of Kondo alloys, i.e., of systems with randomly placed Kondo ions of concentration x. The values of x were ranging from close to $x=0$ (dilute Kondo impurities) to $x=1$ (Kondo lattice). Different hopping matrix elements were assumed depending on whether the initial and final sites are Kondo or nonmagnetic sites. By expressing the spin of a Kondo site in terms of fermionic operators and by making a mean-field approximation we derived a Hamiltonian which has in addition to the conduction band a narrow f band describing the low-energy excitations of the system. The disorder of the system was treated by a (dynamical) coherent potential approximation (CPA) and by a dynamical mean-field theory (DMFT) approach. It was reconfirmed for the special system considered here that both approaches yield identical equations. For a practical application of the formalism a Bethe tree structure was chosen for convenience. It corresponds to working with a semielliptic density of states. Various quantities were calculated as function of the ratio $\alpha=t_{AB}/\sqrt{t_A t_B}$, i.e., of different degrees of off-diagonal disorder and of Kondo ion concentration x. Among them were the local density of states for the Kondo sites (A atoms) and for the nonmagnetic sites (B atoms). They depend strongly on the degree of disorder and on concentration x. Of special interest was the case of diagonal randomness only. In that case $t_A=t_B=t_{AB}$ and $\alpha=1$. The ratio between the two low temperature scales T_0 and T_K was investigated as function of x, i.e., ranging from the impurity to the Kondo lattice limit. This ratio was shown to be of relevance for a number of experiments. Finally, a detailed study was presented for the case of a combined diagonal and off-diagonal disorder. In particular, the behavior of the Kondo temperature as function of x was studied in detail. The same holds true for the ratio

T_0/T_K. The latter can have a strong monotonic behavior as function of x with peaks at different values of x, and depends on the particular filling of the conduction band as well as on the parameter α. Depending on the ratio T_0/T_K we have obtained universal temperature regimes where the system has either properties of a liquid with light fermions and quasifree local moments or of a liquid with heavy quasiparticles. There is also a temperature regime possible with non-Fermi-liquid behavior. A still open question is under which conditions Luttinger's theorem is inapplicable and how one can calculate in that case the volume enclosed by the Fermi surface. As is well known that volume does not include the electrons which form localized moments when we are in the regime of a light Fermi liquid. But they must be included when we are in the regime of heavy quasiparticles. Another open issue is the possibility for the system to reach a magnetic unstability at intermediate concentration of Kondo impurities, due to the RKKY interaction. Under which conditions this unstability might occur, and whereas it would be associated with a long range or to a spin glass ordering are still unanswered questions of experimental and theoretical relevance. Although the present investigation sheds some light on Kondo alloys and their properties there are important issues remaining for the future. For example, as pointed out before, a more systematic experimental study of the crossover for Ce-La and Yb-Lu Kondo alloys is highly desirable.

ACKNOWLEDGMENTS

We would like to thank N. B. Perkins for stimulating discussions during the early phase of this work. We thank M. Vojta for comments which helped us to improve the manuscript. We thank M. Capone, K. Kikoin, M. Laad, and C. Lacroix for fruitful discussions.

APPENDIX: COHERENT POTENTIAL APPROXIMATION EQUATIONS

1. Starting definitions

Considering the mean-field Kondo-alloy model defined by the effective Hamiltonian equation (4), we define the Green's function, transfer integral, and local propagator matrices, as

$$\tilde{\mathbf{G}}_{ij} = \begin{pmatrix} \hat{x}_i\hat{x}_j G_{ij}^{ff} & \hat{x}_i\hat{x}_j G_{ij}^{fc} & \hat{x}_i\hat{y}_j G_{ij}^{fc} \\ \hat{x}_i\hat{x}_j G_{ij}^{cf} & \hat{x}_i\hat{x}_j G_{ij}^{cc} & \hat{x}_i\hat{y}_j G_{ij}^{cc} \\ \hat{y}_i\hat{x}_j G_{ij}^{cf} & \hat{y}_i\hat{x}_j G_{ij}^{cc} & \hat{y}_i\hat{y}_j G_{ij}^{cc} \end{pmatrix}, \quad \tilde{\mathbf{W}} = \begin{pmatrix} 0 & 0 & 0 \\ 0 & t_A & t_{AB} \\ 0 & t_{AB} & t_B \end{pmatrix}, \tag{A1}$$

$$\tilde{\mathbf{\Pi}}_i(i\omega) = \begin{pmatrix} \hat{x}_i \mathbf{\Pi}_A(i\omega) & & 0 \\ & & 0 \\ 0 \quad 0 & & \hat{y}_i/(i\omega+\mu) \end{pmatrix}$$

$$\text{with } \mathbf{\Pi}_A(i\omega) = \begin{pmatrix} i\omega+\lambda & r \\ r & i\omega+\mu \end{pmatrix}^{-1}. \tag{A2}$$

The projection operator $\hat{x}_i = 1-\hat{y}_i$ is unity if i refers to site A, and zero otherwise.

2. Equation of motion

The equations of motion derived from the Hamiltonian equation (4) for the scalar Green's functions G_{ij}^{ff}, G_{ij}^{fc}, and G_{ij}^{cc} can be cast into the following matrix form:

$$\tilde{\mathbf{G}}_{ij}(i\omega) = \tilde{\mathbf{\Pi}}_i(i\omega)\delta_{ij} + \tilde{\mathbf{\Pi}}_i(i\omega)\tilde{\mathbf{W}}\gamma_{ij}\tilde{\mathbf{\Pi}}_j(i\omega) + \sum_l \tilde{\mathbf{\Pi}}_i(i\omega)\tilde{\mathbf{W}}\gamma_{il}\tilde{\mathbf{\Pi}}_l(i\omega)\tilde{\mathbf{W}}\gamma_{lj}\tilde{\mathbf{\Pi}}_j(i\omega) + \cdots. \tag{A3}$$

We assume that the Green's function and local propagator matrices can be inverted. This hypothesis can be satisfied by introducing a nonzero parameter δ such that $\hat{x}_i = 1-\delta$ (or $x_i = \delta$) if i is a site A (a site B). The limit $\delta = 0$ is taken at the end of the calculations. Equation (A3) can then be expressed as

$$(\tilde{\mathbf{G}}^{-1})_{ij}(i\omega) = \tilde{\mathbf{\Pi}}_i^{-1}(i\omega)\delta_{ij} - \tilde{\mathbf{W}}\gamma_{ij}. \tag{A4}$$

3. Local self-energy approximation

Generalizing the CPA procedure of Refs. 13 and 14, we assume that the averaged Green's function matrix is characterized by a local 3×3 self-energy matrix $\tilde{\mathbf{\Sigma}}$,

$$([\tilde{\mathbf{G}}(i\omega)]^{-1})_{ij} = i\omega\tilde{\mathbf{I}}\delta_{ij} - \tilde{\mathbf{\Sigma}}(i\omega)\delta_{ij} - \tilde{\mathbf{W}}\gamma_{ij}, \tag{A5}$$

where $\tilde{\mathbf{I}}$ is the 3×3 identity matrix. Averaging over a random distribution of sites A and B restores the translation symmetry of the underlying lattice. The averaged matrix Green's function is periodic in space, and its Fourier transform is

$$\tilde{\mathbf{G}}_{\mathbf{k}} \equiv \sum_{ij} e^{-i\mathbf{k}\cdot(\mathbf{R}_i-\mathbf{R}_j)}[\tilde{\mathbf{G}}_{ij}]. \tag{A6}$$

Equation (A4) can then be expressed as

$$\tilde{\mathbf{G}}_{\mathbf{k}}^{-1}(i\omega) = i\omega\tilde{\mathbf{I}} - \tilde{\mathbf{\Sigma}}(i\omega) - \tilde{\mathbf{W}}\gamma_{\mathbf{k}}. \tag{A7}$$

Next we establish a complete set of self-consistent equations for the Green's function and the self-energy, whose matrix-elements are parametrized as follows:

$$\tilde{\mathbf{\Sigma}}(i\omega) \equiv \begin{pmatrix} & \mathbf{\Sigma}_A(i\omega) & & \sigma_1(i\omega) \\ & & & \sigma_2(i\omega) \\ \sigma_1(i\omega) & & \sigma_2(i\omega) & \Sigma_B(i\omega) \end{pmatrix} \equiv \begin{pmatrix} \Sigma_A^{ff}(i\omega) & \Sigma_A^{fc}(i\omega) & \sigma_1(i\omega) \\ \Sigma_A^{cf}(i\omega) & \Sigma_A^{cc}(i\omega) & \sigma_2(i\omega) \\ \sigma_1(i\omega) & \sigma_2(i\omega) & \Sigma_B^{cc}(i\omega) \end{pmatrix}. \tag{A8}$$

4. Off-diagonal blocks of $\tilde{\mathbf{\Sigma}}$: No double A-B occupancy

A first set of relations is obtained by expressing the local averaged Green's function in terms of their $\mathbf{k}$-dependent counterparts.

$$[\tilde{\mathbf{G}}_{00}(i\omega)] \equiv \begin{pmatrix} xG_A^{ff}(i\omega) & xG_A^{fc}(i\omega) & 0 \\ xG_A^{cf}(i\omega) & xG_A^{cc}(i\omega) & 0 \\ 0 & 0 & (1-x)G_B^{cc}(i\omega) \end{pmatrix} = \sum_{\mathbf{k}} \tilde{\mathbf{G}}_{\mathbf{k}}(i\omega). \tag{A9}$$

Here $\tilde{\mathbf{G}}_{\mathbf{k}}$ is of the form of Eq. (A7). Even if our approach artificially introduces two conducting bands A and B, the vanishing of the off-diagonal mixed A-B matrix elements in $\langle \tilde{\mathbf{G}}_{00} \rangle_r$ prevents a double association of A and B atoms with the same site. The two corresponding equations determine the self-energy off-diagonal blocks σ_1 and σ_2.

5. Diagonal blocks of $\tilde{\Sigma}$: Scattering of the effective medium

Self-consistent relations for $\mathbf{\Sigma}_A$ and Σ_B are obtained by requiring that the scattering of electrons of the effective medium by a given site vanishes on average. For a given random configuration of the alloy, and using Eqs. (A4) and (A5), the Green's function $\tilde{\mathbf{G}}$, is related to its average by

$$(\tilde{\mathbf{G}}^{-1})_{ij} = ([\tilde{\mathbf{G}}]^{-1})_{ij} - \tilde{\mathbf{v}}_i \delta_{ij}, \tag{A10}$$

where

$$\tilde{\mathbf{v}}_i(i\omega) = i\omega\tilde{\mathbf{I}} - \tilde{\mathbf{\Pi}}_i^{-1}(i\omega) - \tilde{\mathbf{\Sigma}}(i\omega) = \begin{pmatrix} i\omega - \Sigma_A^{ff}(i\omega) - (i\omega+\lambda)/\hat{x}_i & -\Sigma_A^{fc}(i\omega) - r/\hat{x}_i & -\sigma_1(i\omega) \\ -\Sigma_A^{cf}(i\omega) - r/\hat{x}_i & i\omega - \Sigma_A^{cc}(i\omega) - (i\omega+\mu)/\hat{x}_i & -\sigma_2(i\omega) \\ -\sigma_1(i\omega) & -\sigma_2(i\omega) & i\omega - \Sigma_B^{cc}(i\omega) - (i\omega+\mu)/\hat{y}_i \end{pmatrix}. \tag{A11}$$

The single-site scattering T matrix on site i is given by

$$\tilde{\boldsymbol{\tau}}_i = (\tilde{\mathbf{I}} - \tilde{\mathbf{v}}_i[\tilde{\mathbf{G}}_{ii}])^{-1}\tilde{\mathbf{v}}_i \tag{A12}$$

$$= (\tilde{\mathbf{v}}_i^{-1} - [\tilde{\mathbf{G}}_{ii}])^{-1}. \tag{A13}$$

As mentioned above, the required matrix inversions can be performed by introducing a nonzero parameter δ such that $\hat{x}_i$ is equal to $1-\delta$ (site A) or δ (site B). We now consider the limit $\delta=0$ and we express the scattering matrices $\tilde{\boldsymbol{\tau}}_A$ and $\tilde{\boldsymbol{\tau}}_B$ on a site A (B). We find

$$\tilde{\boldsymbol{\tau}}_A = \begin{pmatrix} (\mathbf{v}_A^{-1} - x\mathbf{G}_A)^{-1} & 0 \\ 0 \quad 0 & -[(1-x)G_B^{cc}]^{-1} \end{pmatrix}, \tag{A14}$$

and

$$\tilde{\boldsymbol{\tau}}_B = \begin{pmatrix} -(x\mathbf{G}_A)^{-1} & 0 \\ 0 \quad 0 & [v_B^{-1} - (1-x)G_B^{cc}]^{-1} \end{pmatrix}, \tag{A15}$$

with

$$\mathbf{v}_A(i\omega) = -\begin{pmatrix} \lambda & r \\ r & \mu \end{pmatrix} - \mathbf{\Sigma}_A(i\omega), \tag{A16}$$

$$\mathbf{G}_A(i\omega) = \begin{pmatrix} G_A^{ff}(i\omega) & G_A^{fc}(i\omega) \\ G_A^{cf}(i\omega) & G_A^{cc}(i\omega) \end{pmatrix}, \tag{A17}$$

$$v_B(i\omega) = -\mu - \Sigma_B(i\omega). \tag{A18}$$

We obtain the CPA equations for $\mathbf{\Sigma}_A$ and Σ_B by setting $[\tilde{\boldsymbol{\tau}}_i] = x\tilde{\boldsymbol{\tau}}_A + (1-x)\tilde{\boldsymbol{\tau}}_B = 0$. The result is

$$\mathbf{\Sigma}_A(i\omega) = -\begin{pmatrix} \lambda & r \\ r & \mu \end{pmatrix} - \frac{(1-x)}{x}\mathbf{G}_A^{-1}(i\omega),$$

$$\Sigma_B(i\omega) = -\mu - \frac{x}{(1-x)G_B^{cc}(i\omega)}. \tag{A19}$$

[1] P. Fulde, P. Thalmeier, and G. Zwicknagl, *Strongly Correlated Electrons*, Solid State Physics Vol. 60 (Elsevier, New York, 2006).

[2] G. R. Stewart, Rev. Mod. Phys. **73**, 797 (2001).

[3] A. C. Hewson, *The Kondo Problem to Heavy Fermions* (Cambridge University Press, Cambridge, 1993).

[4] J. R. Schrieffer and P. A. Wolf, Phys. Rev. **149**, 491 (1966).

[5] V. Dobrosavljevic, T. R. Kirkpatrick, and G. Kotliar, Phys. Rev. Lett. **69**, 1113 (1992).

[6] E. Miranda, V. Dobrosavljevic, and G. Kotliar, Phys. Rev. Lett. **78**, 290 (1997).

[7] S. Kettemann and E. R. Mucciolo, JETP Lett. **83**, 240 (2006).

[8] K. Byczuk, W. Hofstetter, and D. Vollhardt, Phys. Rev. Lett. **94**, 056404 (2005).

[9] A. M. Sengupta and A. Georges, Phys. Rev. B **52**, 10295 (1995).
[10] A. H. Castro Neto, G. Castilla, and B. A. Jones, Phys. Rev. Lett. **81**, 3531 (1998).
[11] S. Burdin, D. R. Grempel, and A. Georges, Phys. Rev. B **66**, 045111 (2002).
[12] R. K. Kaul and M. Vojta, Phys. Rev. B **75**, 132407 (2007).
[13] J. A. Blackman, D. M. Esterling, and N. F. Berk, Phys. Rev. B **4**, 2412 (1971).
[14] D. M. Esterling, Phys. Rev. B **12**, 1596 (1975).
[15] A. Georges, G. Kotliar, W. Krauth, and M. J. Rozenberg, Rev. Mod. Phys. **68**, 13 (1996).
[16] W. Metzner and D. Vollhardt, Phys. Rev. Lett. **62**, 324 (1989).
[17] C. Lacroix and M. Cyrot, Phys. Rev. B **20**, 1969 (1979).
[18] B. Coqblin, M. A. Gusmao, J. R. Iglesias, C. Lacroix, A. Ruppenthal, and A. S. D. Simoes, Physica B **282**, 50 (2000).
[19] N. Read, D. M. Newns, and S. Doniach, Phys. Rev. B **30**, 3841 (1984).
[20] D. M. Newns and N. Read, Adv. Phys. **36**, 799 (1987).
[21] P. Coleman, Phys. Rev. B **35**, 5072 (1987).
[22] See, for example, P. Fulde, *Electron Correlations in Molecules and Solids*, Springer Series in Solid State Sciences, 3rd enlarged ed. (Springer-Verlag, Berlin, 1995).
[23] P. Soven, Phys. Rev. **156**, 809 (1967).
[24] D. W. Taylor, Phys. Rev. **156**, 1017 (1967).
[25] B. Velicky, S. Kirkpatrick, and H. Ehrenreich, Phys. Rev. **175**, 747 (1968).
[26] H. Hasegawa and J. Kanamori, J. Phys. Soc. Jpn. **31**, 382 (1971).
[27] S. Burdin, A. Georges, and D. R. Grempel, Phys. Rev. Lett. **85**, 1048 (2000).
[28] M. Jarrell and H. R. Krishnamurthy, Phys. Rev. B **63**, 125102 (2001).
[29] Y. Kakehashi, Phys. Rev. B **66**, 104428 (2002).
[30] A. Chattopadhyay, S. Das Sarma, and A. J. Millis, Phys. Rev. Lett. **87**, 227202 (2001).
[31] M. Jarrell, H. Akhlaghpour, and T. Pruschke, Phys. Rev. Lett. **70**, 1670 (1993).
[32] A. N. Tahvildar-Zadeh, M. Jarrell, and J. K. Freericks, Phys. Rev. Lett. **80**, 5168 (1998).
[33] Th. Pruschke, R. Bulla, and M. Jarrell, Phys. Rev. B **61**, 12799 (2000).
[34] N. Andrei, Phys. Rev. Lett. **45**, 379 (1980).
[35] P. Wiegman, JETP Lett. **31**, 392 (1980).
[36] P. Nozières, Ann. Phys. (Paris) **10**, 19 (1985).
[37] P. Nozières, Eur. Phys. J. B **6**, 447 (1998).
[38] P. Nozières, J. Phys. Soc. Jpn. **74**, 4 (2005).
[39] T. Costi and N. Manini, J. Low Temp. Phys. **126**, 835 (2002).
[40] E. D. Bauer, C. H. Booth, J. M. Lawrence, M. F. Hundley, J. L. Sarrao, J. D. Thompson, P. S. Riseborough, and T. Ebihara, Phys. Rev. B **69**, 125102 (2004).
[41] R. Mallik, E. V. Sampathkumaran, P. L. Paulose, J. Dumschat, and G. Wortmann, Phys. Rev. B **55**, 3627 (1997).
[42] E. D. Mun, Y. S. Kwon, and M. H. Jung, Phys. Rev. B **67**, 033103 (2003).
[43] C. L. Lin, A. Wallash, J. E. Crow, T. Mihalisin, and P. Schlottmann, Phys. Rev. Lett. **58**, 1232 (1987).
[44] S. Burdin and V. Zlatic, arXiv:cond-mat/0212222 (unpublished).